Energetic stability and magnetic coupling in $(Cr_{1-x}Fe_x)_2O_3$: Evidence for a ferrimagnetic ilmenite-type superlattice from first principles

Hasan Sadat Nabi and Rossitza Pentcheva*

Department of Earth and Environmental Sciences and Center of Nanoscience (CENS), University of Munich, Theresienstr. 41, 80333 Munich, Germany

(Received 23 February 2011; revised manuscript received 3 May 2011; published 16 June 2011)

Based on density functional theory (DFT) calculations with a Hubbard U-term, we explore the possibility to design an artificial ferrimagnet $FeCrO_3$ of ilmenite type out of the two antiferromagnets α-Fe_2O_3 and α-Cr_2O_3. By varying the concentration of Fe in α-Cr_2O_3, we provide a phase diagram of the relative stability of different chemical and magnetic arrangements with respect to the end members. At 50% Fe-doped α-Cr_2O_3, the ilmenite-like structure with alternating Fe and Cr layers and antiparallel magnetic moments competes energetically with a phase-separated structure containing a mixed Fe-Cr interface layer. The magnetic interaction parameters between Fe($3d^5$) and Cr($3d^3$) ions in the digital ferrimagnetic heterostructure, extracted by mapping the DFT total energies to a Heisenberg Hamiltonian, indicate a hematite-like magnetic order with parallel intralayer and antiparallel interlayer alignment.

DOI: 10.1103/PhysRevB.83.214424 PACS number(s): 75.30.Et, 75.70.Cn, 75.47.Lx, 73.20.−r

I. INTRODUCTION

The growth of heterostructures containing transition metal oxides is a powerful tool not only to combine different functional properties in one composite material but also to achieve novel electronic states that do not exist in the parent compounds. Unexpected behavior can be driven by a polar discontinuity at the interface, as in the case of the quasi two-dimensional electron gas arising at the interface of the band insulators $LaAlO_3$ and $SrTiO_3$.[1] A further example along the same line is the room-temperature remanent magnetization in nanoscale exsolutions of the antiferromagnets hematite (α-Fe_2O_3) and ilmenite ($FeTiO_3$).[2] DFT calculations[3] have recently provided theoretical evidence that a mixed Fe^{2+}, Fe^{3+} layer forms at the interface and thereby gives rise to uncompensated magnetic moments.

However, novel behavior can be achieved even without a valence discontinuity. To this end, the possibility for a ferro- or ferrimagnetic coupling in perovskite superlattices of $LaCrO_3$ and $LaFeO_3$ (both G-type antiferromagnets) is a matter of debate both experimentally[4,5] and theoretically.[6–8] While most of the scientific interest so far is directed at materials with the perovskite structure, we propose here a ferrimagnetic d^3-d^5 system with a corundum-derived structure built out of the two antiferromagnets α-Fe_2O_3 and α-Cr_2O_3. In the corundum structure, oxygen forms a distorted hcp lattice and cations occupy 2/3 of the octahedral sites. Despite the similar structure, hematite (α-Fe_2O_3) and eskolaite (Cr_2O_3) have a different magnetic ordering: In hematite ($T_N \sim 950$ K), Fe^{3+}-ions are coupled ferromagnetically (FM) within the layer and antiferromagnetically to adjacent layers along the [0001]-direction. In contrast, in eskolaite ($T_N \sim 307$ K), Cr^{3+}-ions have antiferromagnetic (AFM) intralayer coupling. In the proposed ilmenite-like $FeCrO_3$ system with alternating Fe and Cr layers, the angle between Cr-O-Fe in corner sharing octahedra ranges from 120° to 135° which according to the Goodenough-Kanamori (GK) rules[9,10] leads to an antiferromagnetic coupling.[9] However, the different sizes of the local moments on Fe and Cr result in a net magnetization of $2\mu_B$ per Fe-Cr pair and thus ferrimagnetism. In contrast, the Cr-O-Fe angle of 180° in the double perovskite $LaCrO_3$/$LaFeO_3$ superlattices is expected to cause a ferromagnetic coupling after the GK rules.

$FeCrO_3$ is a member of the $(Cr_{1-x}Fe_x)_2O_3$ series which has diverse applications in catalysis and gas sensing[11–13] and also occurs on the surface of stainless steels.[14,15] The cation distribution turns out to be strongly dependent on the synthesis conditions and is a matter of controversy: x-ray and neutron powder diffraction studies reported a continuous solid solution series over the entire concentration range (e.g., Refs. 16–18) at temperatures above 1200 K, but there are indications for phase separation into Cr_2O_3- and Fe_2O_3-rich regions for $x = 40\%$–80% at lower temperatures.[19–21] On the other hand, infrared and Raman spectra[17,22] are interpreted as evidence for cation ordering in an ilmenite-type lattice (alternating layers of Fe and Cr). Theoretically, the thermodynamics of $(Cr_{1-x}Fe_x)_2O_3$ has been addressed so far by molecular dynamics simulations with classical interatomic potentials.[23] This study found close competition between various cation distributions and also addressed the role of magnetic interactions by adding a model Hamiltonian with estimated interaction parameters. A previous DFT study with hybrid functionals (B3LYP) concentrated mainly on antiferromagnetic configurations at the concentration of $x = 50\%$ (Ref. 24) in a rhombohedral setup (10 atoms in the unit cell). Isolated Cr impurities in α-Fe_2O_3 were studied by Velev *et al.*[25]

Here, we explore the stability and magnetic coupling in $(Cr_{1-x}Fe_x)_2O_3$ as a function of the Fe-doping concentration x using DFT calculations including an on-site Coulomb repulsion term (LDA/GGA + U method[26]). We have used a hexagonal setup with 30 atoms in the unit cell which provides a larger freedom to vary the concentration, chemical and magnetic ordering. In order to resolve the controversy concerning the cation distribution, we determine the relative stability of solid solutions, cation ordered (layered), and phase-separated configurations. The main goal of this study is to investigate how the magnetic coupling evolves with Fe concentration and arrangement and most importantly, whether a digital superlattice with ferrimagnetic order can be stabilized.

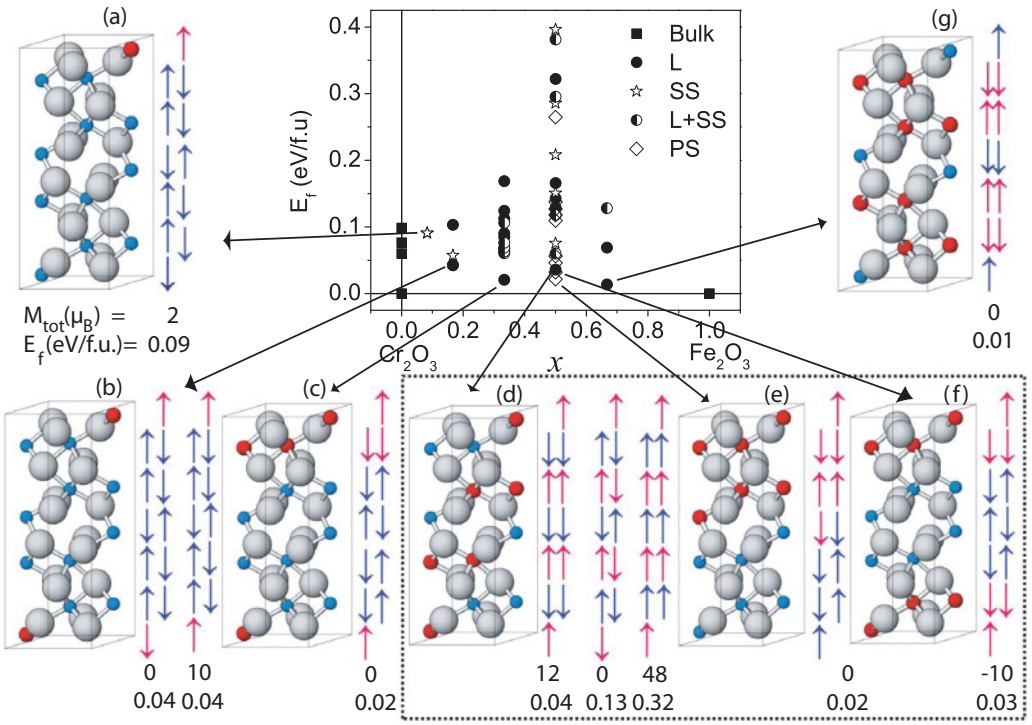

FIG. 1. (Color online) The formation energy (eV/f.u.) as a function of Fe concentration x for $(Cr_{1-x}Fe_x)_2O_3$ using $U = 4.5$ and $J = 1$ eV for the Cr and Fe $3d$ states. The filled squares correspond to different magnetic arrangements of the bulk end members. Filled circles mark layered configurations (L). The open stars refer to solid solutions (SS) and the half-filled symbols denote layered configurations with a mixed interface (L + SS). Phase-separated configurations (PS) are marked by open diamonds for the concentration of $x = 0.5$. Additionally, several of the most stable chemical and spin configurations are displayed together with the respective total magnetic moment and formation energy. Fe, Cr and oxygen ions are denoted by red (dark gray) and small blue (gray) and large light gray spheres, respectively.

To shed more light on the nature of magnetic coupling, the exchange interaction parameters of the digital $FeCrO_3$ superlattice are extracted from the DFT total energies and compared to those of the end members.

II. CALCULATIONAL DETAILS

The calculations are performed with the all-electron full-potential linearized augmented plane wave (FP-LAPW) method as implemented in the WIEN2K code.[27] It is well known that the generalized gradient approximation (GGA) (Ref. 28) for the exchange correlation functional significantly underestimates the band gaps of these transition metal oxides.[29] To reproduce correctly the experimental band gaps of Fe_2O_3 [2.2 eV (Refs. 30 and 31)] and Cr_2O_3 [3.4 eV Refs. 32 and 33)], we used an additional on-site Coulomb interaction[26] term with $U = 6.0$ and 4.5 eV ($J = 1.0$ eV) for Fe- and Cr $3d$ states, respectively. Tests with U values, ranging from 4.5 to 8 eV, showed that the trend in the energetic stability is not affected by the U value.

The muffin tin (MT) radii are fixed to 1.80 bohr (Fe and Cr) and 1.60 bohr (oxygen). Inside the muffin tins, wave functions are expanded in spherical harmonics up to $l_{\max}^{\mathrm{wf}} = 10$ and nonspherical contributions to the electron density and potential are considered up to $l_{\max}^{\mathrm{pot}} = 6$. The energy cutoff for the plane wave representation in the interstitial is $E_{\max}^{\mathrm{wf}} = 25$ Ry for the wave functions and $E_{\max}^{\mathrm{pot}} = 196$ Ry for the potential. A total of 100 k-point (16 k-points in the irreducible part of Brillouin zone) is used for the integration in reciprocal space. The convergence criteria ensure a numerical accuracy of energy differences of 0.01 mRy/f.u. (f.u. = formula unit).

The structures are simulated in a hexagonal setup with 30 atoms/unit cell. Some of the configurations are displayed in Fig. 1. The lattice parameters of the intermediate members are set to those of α-Cr_2O_3 optimized within GGA + U ($a^{\mathrm{th}} = 5.06$ Å, $c^{\mathrm{th}} = 13.86$ Å). These are ~2% larger than the experimental values for α-Cr_2O_3 [$a = 4.96$ Å, $c = 13.60$ Å (Ref. 34)], but consistent with previous GGA + U (Ref. 35) and B3LYP calculations.[24] Changing the lattice parameters to the experimental values of eskolaite or hematite [$a = 5.04$ Å, $c = 13.75$ Å (Ref. 36)] did not influence the energetic trends. For all configurations, the internal degrees of freedom are fully relaxed.[37]

III. RESULTS AND DISCUSSION

A. Energetic stability and magnetic order

To investigate the energetic stability, we have varied the Fe concentration from 0% to 100% and thereby considered more than 45 different chemical and magnetic arrangements, including solid solutions, layered arrangements (e.g., ilmenite type) and phase-separated configurations (cf. Fig. 1). The formation energy of each system with respect to bulk Cr_2O_3 and Fe_2O_3 is defined as $E_f = E_{(Cr_{1-x}Fe_x)_2O_3} - (1-x)E_{Cr_2O_3} - xE_{Fe_2O_3}$, where $E_{(Cr_{1-x}Fe_x)_2O_3}$, $E_{Cr_2O_3}$, and $E_{Fe_2O_3}$ are the total energies of the intermediate and the two end members, respectively.

Several exemplary configurations and magnetic arrangements with their corresponding total magnetic moments and formation energies are displayed in addition to the phase diagram in Fig. 1.

For low Fe-concentration (e.g., 16%), the formation of an iron layer in the Cr_2O_3 host [Fig. 1(b)] is favored over a solid solution (SS) with mixed Fe-Cr layers. In the configuration shown in Fig. 1(b), the Cr_2O_3 host preserves the bulk magnetic coupling of eskolaite, characterized by an AFM arrangement within the layer. In the Fe layer, however, the parallel and antiparallel alignments between the Fe ions are energetically degenerate.

With increasing Fe concentration and in particular for 50% Fe-doped eskolaite, there is a strong competition between the layered ilmenite-like [Fig. 1(d)] and the phase-separated systems with a hematite and eskolaite block [Figs. 1(e) and 1(f)]. In the latter two, each block obtains the magnetic ordering of the corresponding end member. In the configuration shown in Fig. 1(e), a FM coupling in the mixed (Fe, Cr)-interface layer is favored by 0.02 eV/f.u. compared to AFM coupling. Solid solutions, modeled by mixed Fe, Cr layers (not shown in Fig. 1) are energetically less stable: the most favorable SS-configuration has the hematite magnetic structure and is 0.08 eV/f.u. less favorable, while a configuration with the eskolaite magnetic structure is 0.15 eV less favorable. Interestingly, in the digital ilmenite-like $FeCrO_3$ structure [Fig. 1(d)], a FM coupling within the layer and an AFM alignment to the next layer (as in hematite bulk) is energetically favored by 0.1 eV/f.u. over a magnetic structure analogous to eskolaite and by 0.3 eV/f.u. over a fully ferromagnetically coupled system. These relatively large energy differences between different magnetic arrangements indicate the dominant role of magnetic coupling in the stabilization of this system, as previously suggested based on a model Hamiltonian for the magnetic interactions.[23] In the most stable magnetic configuration of the ilmenite-like $FeCrO_3$ [Fig. 1(d)], FM aligned Cr layers ($3d^3$) couple antiparallel to Fe layers ($3d^5$). The different sizes of magnetic moments on Cr^{3+} (GGA + U value: 2.4 μ_B) and Fe^{3+} (GGA + U value: 4.2 μ_B) result in a ferrimagnetic structure with a net magnetic moment of 12 μ_B per 30 atoms unit cell. Beyond 50%, the magnetic structure of hematite (ferromagnetic intralayer and AFM interlayer arrangement) is adopted for layered configurations [Fig. 1(g)]. The phase diagram (Fig. 1) illustrates the transition of magnetic ordering from the one in eskolaite to the one in hematite with increasing Fe content.

B. Electronic properties and band alignment

The electronic properties of the ferrimagnetic ilmenite-like configuration of $FeCrO_3$ are analyzed in Fig. 2. Fe_2O_3 is a charge transfer type of insulator with a band gap of 2.2 eV (Refs. 30 and 31) between occupied O2p and an empty Fe3d upper Hubbard band, whereas Cr_2O_3 is a mixed charge transfer and Mott-Hubbard type of insulator. Its band gap of 3.4 eV (Refs. 32 and 33) is defined by occupied O2p and Cr t_{2g} and empty Cr e_g states. The layered $FeCrO_3$ system possesses also a mixed type of band gap; however, the valence band maximum (VBM) is determined by occupied O2p and Cr t_{2g} as in Cr_2O_3, while the conduction band minimum (CBM) is

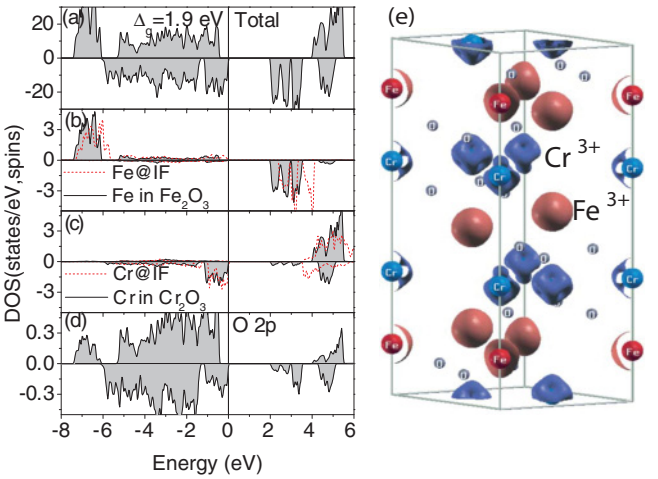

FIG. 2. (Color online) (a) Total and (b–d) projected density of states (DOS) for the layered $FeCrO_3$ structure [see Figs. 1(d) and 1(e)], the corresponding spin density displays the characteristic orbital occupation of Fe^{3+} ($3d^5$, red/light gray) and Cr^{3+} ($3d^3$ with occupied t_{2g} orbitals shown in blue/dark gray).

formed by Fe3d states as in Fe_2O_3. As the latter lie lower than the unoccupied Cr states, the band gap of $FeCrO_3$ is reduced to 1.9 eV. Furthermore, the Fe 3d upper (as well as lower) Hubbard band is slightly narrower compared to that of bulk Fe_2O_3 [see Fig. 2(b)] and shifted to lower energies. A narrowing of the upper Hubbard band is observed also for Cr [see Fig. 2(c)], indicating a reduced hybridization in $FeCrO_3$.

Similar sizes of the band gaps are obtained for the other stable phase-separated configurations in Figs. 1(e) and 1(f). To investigate the band alignment across the interface, we have plotted in Fig. 3 the layer-resolved DOS for these two configurations. In both cases, the CBM is defined by the Fe3d band in the Fe_2O_3 block and the VBM by O2p and Cr t_{2g} states at the Cr_2O_3 part. However, the configuration with a mixed Fe, Cr interface layer [Fig. 1(e)] shows a stronger offset of the VBM across the interface (the O2p band in the Fe_2O_3 part lies ∼0.4 eV lower than the O2p states in

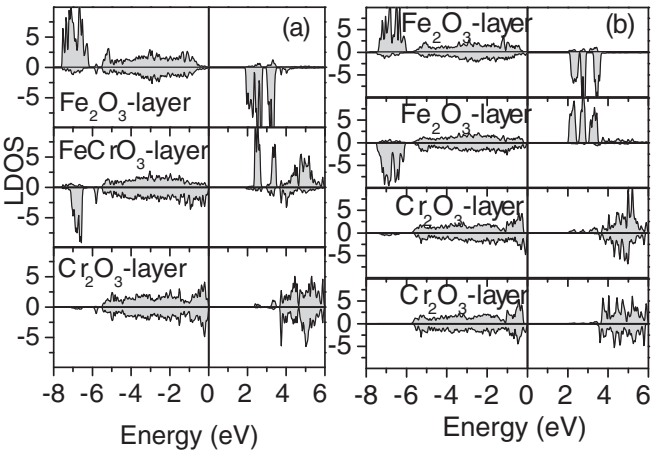

FIG. 3. Layer-resolved density of states for the phase-separated configurations displayed in (a) [Fig. 1(e)] and (b) [Fig. 1(f)], respectively.

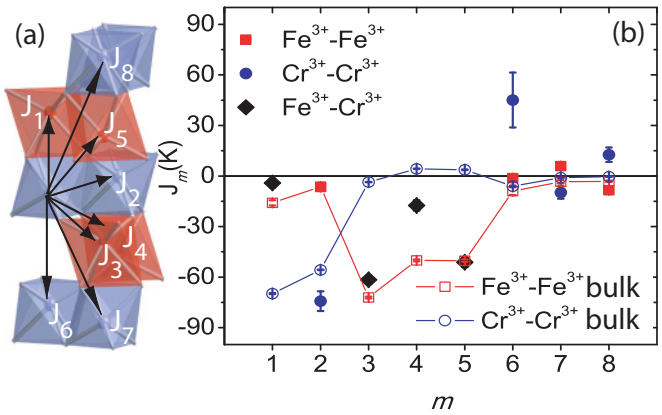

FIG. 4. (Color online) (a) Magnetic pair interaction parameters $[J_m^q(K)]$ in the corundum structure. (b) Values of $J_m^q(K)$ for $FeCrO_3$ (filled symbols) are compared to the ones for bulk hematite (Fe^{3+}-Fe^{3+}) and eskolaite (Cr^{3+}-Cr^{3+}) shown with open symbols. For Cr (Fe) $3d$ states $U = 4.5(6.0)$ and $J = 1$ eV was used. $J^q < 0$ (>0) corresponds to antiferromagnetic (ferromagnetic) coupling.

the Cr_2O_3 part). Such an asymmetry in the band offset in α-Fe_2O_3-α-Cr_2O_3 heterostructures has been addressed recently both experimentally[38] and by GGA calculations.[39] In the latter, however, the band gaps are significantly underestimated, which is likely to affect the band alignment.

The spin density plot in Fig. 2(e) shows the antiparallel arrangement of Fe^{3+} ($3d^5$) and Cr^{3+} ($3d^3$) in the ilmenite-like $FeCrO_3$ and their orbital occupation: The red (light gray) spheres correspond to the half-filled d-band of Fe^{3+} in the majority spin channel, while the characteristic shapes of filled t_{2g} orbitals of Cr^{3+} in the minority spin channel are shown in blue (dark gray).

C. Magnetic exchange interaction parameters

In order to gain more insight into the magnetic coupling of the artificially layered $FeCrO_3$ system, we have extracted its magnetic interaction parameters and compared those to the ones in the end members, Fe_2O_3 and Cr_2O_3. The magnetic exchange interaction parameters J_{ij}^q between the spins on site i and j are obtained by mapping total energies of different spin configurations onto a Heisenberg Hamiltonian. The latter is defined as $H = H_0 - \frac{1}{2}\sum_{i,j} J_{ij}^q \mathbf{S}_i \cdot \mathbf{S}_j$, where $\mathbf{S}_i$ is the spin vector at lattice site i with S = 3/2 and 5/2 for Cr^{3+} and Fe^{3+}, respectively. The superscript q denotes the type of cation pairs (Fe^{3+}-Fe^{3+}, Cr^{3+}-Cr^{3+}, or Fe^{3+}-Cr^{3+}). For more details see Ref. 40. The distinct interaction parameters J_m with $(ij) = m$ are illustrated in Fig. 4(a).

As shown in Fig. 4(b), in hematite (open squares), the dominant magnetic interaction is the antiferromagnetic coupling between Fe ions in corner sharing octahedra in neighboring layers ($J_3 \sim -72$ K, $J_4 = J_5 \sim -50$ K with $U = 6$ eV). The calculated values are in good agreement with values obtained from inelastic neutron scattering data.[41] In contrast, in Cr_2O_3 (open circles), the magnetic structure is determined by a strong antiferromagnetic interaction between cations in face and edge sharing octahedra $J_1 \sim -70$ K and $J_2 \sim -56$ K, consistent with previous DFT calculations.[42] The different magnetic structure of Fe_2O_3 and Cr_2O_3 arises from the difference in orbital occupation: for Fe^{3+} ($3d^5$) the antiferromagnetic superexchange in corner sharing octahedra via $p\sigma$ orbitals dominates, while in Cr_2O_3 (Cr^{3+}: t_{2g}^3, e_g^0) the d^3-d^3 interaction proceeds mainly via $p\pi$ bonding and direct interaction in edge sharing octahedra.

The magnetic interaction parameters in the $FeCrO_3$ superlattice are extracted using 21 different spin arrangements. Because the structure consists of alternating Fe and Cr layers, the interaction parameters J_2, J_6, J_7, and J_8 exist only between Fe-Fe and Cr-Cr pairs. Overall, they show similar behavior to the corresponding interaction in α-Fe_2O_3 or α-Cr_2O_3 bulk: The intralayer interaction is weakly antiferromagnetic for Fe pairs ($J_2^{Fe^{3+}\text{-}Fe^{3+}} \sim -7$ K) and strongly antiferromagnetic coupling for Cr pairs ($J_2^{Cr^{3+}\text{-}Cr^{3+}} \sim -74$ K), respectively, analogous to the bulk end members. Due to the long distance to Fe (Cr) ions from the second nearest layer, the magnetic interaction parameters J_6, J_7, and J_8 are relatively small (~10 K).[43]

The magnetic interaction parameters between Cr^{3+} and Fe^{3+} ($J_{1,3,4,5}^{Fe^{3+}\text{-}Cr^{3+}}$) in the heterostructure are predicted to be of antiferromagnetic type. J_1 has the same sign and is similar in strength to the one in hematite indicating a weak antiferromagnetic direct interaction between Cr^{3+} and Fe^{3+} within the face sharing octahedra in accordance with the GK rule for a 90° d^5-d^3 interaction. The prevailing interactions are $J_3^{Fe^{3+}\text{-}Cr^{3+}} \sim -62$, $J_4^{Fe^{3+}\text{-}Cr^{3+}} \sim -17$, and $J_5^{Fe^{3+}\text{-}Cr^{3+}} \sim -51$ K. J_3, J_4, and J_5 indicate a strong antiferromagnetic superexchange through corner sharing octahedra as in hematite. Indeed the GK rules[9,10] suggest a tendency toward an antiferromagnetic coupling for a d^5-d^3 configuration with intermediate cation-oxygen-cation angles. We note that the Cr-O-Fe angles for J_3, J_4, and J_5 are 120°, 130°, and 135°, respectively. In contrast, for an angle of ~180° (as e.g., in the La_2FeCrO_6 double perovskite), the interaction is expected to the ferromagnetic. Still, as recently pointed out by Miura and Terakura,[8] in this case, there is a strong competition between the $pd\pi$ hybridization leading to a AFM arrangement and the $pd\sigma$ coupling leading to a FM state. We conclude that the $FeCrO_3$ superlattice has a magnetic structure analogous to hematite determined by a strong interlayer antiferromagnetic coupling and parallel alignment of cations within the layers. This result supports recent findings from neutron diffraction experiments.[18]

IV. CONCLUSIONS

Using DFT calculations with an on-site Hubbard U-term, we have investigated the electronic and magnetic properties of Fe-doped Cr_2O_3. The results indicate that especially at $x = 50\%$, the phase separation into a hematite and eskolaite block competes strongly with the formation of an ilmenite-like $FeCrO_3$ structure. In the phase-separated system with a mixed Fe-Cr interface layer, the magnetic coupling between Fe and Cr is ferromagnetic resulting in a finite magnetization of the sample. In the ilmenite-like $FeCrO_3$ superlattice, a magnetic order with antiparallel coupling in neighboring Fe and Cr layers, and FM coupling within the layers is most stable. We recall the Fe_2O_3-$FeTiO_3$ heterostructures where ferrimagnetism is induced due to the polar discontinuity at the interface which results in the formation of a mixed Fe^{2+}, Fe^{3+} layer.[2,3,40] In

contrast, in $FeCrO_3$ ferrimagnetism arises due to the different sizes of magnetic moments of Fe^{3+} ($3d^5$) and Cr^{3+} ($3d^3$) in alternating layers. The magnetic interaction parameters extracted from the DFT total energies reveal that the dominant magnetic interaction is the antiparallel coupling between Fe^{3+} and Cr^{3+} in corner sharing octahedra from neighboring layers. In the artificial $FeCrO_3$ superlattice, the conduction band minimum is determined by Fe3*d* states which reduces the band gap from 3.4 eV in Cr_2O_3 to ∼1.9 eV in $FeCrO_3$. The ilmenite-like $FeCrO_3$ bears analogies to $LaCrO_3$-$LaFeO_3$ (Refs. 4–8) and is an example how heterostructuring can be used to design materials with novel functionalities. Despite strong energetic competition to phase-separated arrangements and solid solutions, the predicted ferrimagnetic ilmenite-type $FeCrO_3$ is likely to be realized using state-of-the-art nonequilibrium growth techniques such as molecular beam epitaxy or pulsed laser deposition.

ACKNOWLEDGMENTS

Funding by the DFG (Pe883/4-1), ESF (EuroMinSci), and SFB/TR80 (Project C3), as well as computational time at the Leibniz Rechenzentrum are gratefully acknowledged.

*pentcheva@lrz.uni-muenchen.de

[1] A. Ohtomo and H. Y. Hwang, Nature (London) **427**, 423 (2004).
[2] P. Robinson, R. J. Harrison, S. A. McEnroe, and R. B. Hargraves, Nature **418**, 517 (2002).
[3] R. Pentcheva and H. Sadat Nabi, Phys. Rev. B **77**, 172405 (2008).
[4] K. Ueda, H. Tabata, and T. Kawai, Science **280**, 1064 (1998).
[5] B. Gray, H. N. Lee, J. Liu, J. Chakhalian, and J. W. Freeland, Appl. Phys. Lett. **97**, 013105 (2010).
[6] W. E. Pickett, Phys. Rev. B **57**, 10613 (1998).
[7] W. E. Pickett, Science **281**, 1571a (1998).
[8] K. Miura and K. Terakura, Phys. Rev. B **63**, 104402 (2001).
[9] J. B. Goodenough, Phys. Rev. **117**, 1442 (1960).
[10] J. Kanamori, J. Phys. Chem. Solids **10**, 87 (1959).
[11] C. Rhodes, G. J. Hutchings, and A. M. Ward, Catal. Today **23**, 43 (1995).
[12] Y. Lei, N. W. Cant, and D. L. Trimm, J. Catal. **239**, 227 (2006).
[13] C. Rhodes, B. Peter Williams, F. King, and G. Hutchings, J. Catal. Commun. **3**, 381 (2002).
[14] S. Joseph, G. Venkateswaran, and P. N. Moorthy, J. Nucl. Sci. Technol. **36**, 798 (1999).
[15] J. Manjanna and G. Venkateswaran, Ind. Eng. Chem. Res. **41**, 3053 (2002).
[16] P. Tsokov, V. Blaskov, D. Klissurski, and I. Tsolovski, J. Mater. Sci. **28**, 184 (1993).
[17] K. F. McCarty and D. R. Boehme, J. Solid State Chem. **79**, 19 (1989).
[18] T. Grygar, P. Bezdička, J. Dědeček, E. Petrovsky, and O. Schneeweis, Ceramics-Silikáty **47**, 32 (2003).
[19] S. Musić, M. Lenglet, S. Popović, B. Hannoyer, I. Czakó-Nagy, M. Ristić, D. Balyar, and F. Gashi, J. Mater. Sci. **31**, 4067 (1996).
[20] M. Lenglet, F. Hochu, and S. Musić, Solid State Commun. **94**, 211 (1995).
[21] Y. Murakami, A. Sawata, and Y. Tsuru, J. Mater. Sci. **34**, 951 (1999).
[22] G. Busca, G. Ramis, M. del Carmen Prieto, and V. S. Escribano, J. Mater. Chem. **3**, 665 (1993).
[23] S. Benny, R. Grau-Crespo, and N. H. de Leeuw, Phys. Chem. Chem. Phys. **11**, 808 (2009).
[24] E. A. Moore, Phys. Rev. B **76**, 195107 (2007).
[25] J. Velev, A. Bandyopadhyay, W. H. Butler, and S. J. Sarker, Phys. Rev. B **71**, 205208 (2005).
[26] V. I. Anisimov, I. V. Solovyev, M. A. Korotin, M. T. Czyżyk, and G. A. Sawatzky, Phys. Rev. B **48**, 16929 (1993).
[27] P. Blaha, K. Schwarz, G. K. H. Madsen, D. Kvasnicka, and J. Luitz, *WIEN2k: An Augmented Plane Wave+Local Orbitals Program for Calculating Crystal Properties* (Techn. Universität Wien, Austria, 2001), ISBN 3-9501031-1-2.
[28] J. P. Perdew, K. Burke, and M. Ernzerhof, Phys. Rev. Lett. **77**, 3865 (1996).
[29] A. Rohrbach, J. Hafner, and G. Kresse, Phys. Rev. B **70**, 125426 (2004).
[30] S. Mochizuki, Phys. Status Solidi A **41**, 591 (1977).
[31] D. Benjelloun, J. P. Bonnet, J. P. Doumerc, J. C. Launay, M. Onillon, and P. Hagenmuller, Mater. Chem. Phys. **10**, 503 (1984).
[32] R. Zimmermann, P. Steiner, and S. Hüfner, J. Electron Spectrosc. Relat. Phenom. **78**, 49 (1996).
[33] T. Uozumi, K. Okada, A. Kotani, R. Zimmerman, P. Steiner, S. Hüfner, Y. Tezuka, and S. Shin, J. Electron Spectrosc. Relat. Phenom. **83**, 9 (1997).
[34] M. Baster, F. Bourée, A. Kowalska, and Z. Latacz, J. Alloys Compd. **296**, 1 (2000).
[35] J. Muscat, A. Wander, and N. M. Harrison, Chem. Phys. Lett. **342**, 397 (2001).
[36] D. A. Perkins and J. P. Attfield, J. Chem. Soc. Chem. Commun. **4**, 229 (1991).
[37] F. Tran, J. Kuneš, P. Novak, P. Blaha, and L. D. Marks, Comput. Phys. Commun. **179**, 784 (2008).
[38] S. A. Chambers, Y. Liang, and Y. Gao, Phys. Rev. B **61**, 13223 (2000).
[39] J. E. Jaffe, M. Dupuis, and M. Gutowski, Phys. Rev. B **69**, 205106 (2004).
[40] H. Sadat Nabi, R. Pentcheva, and R. J. Harrison, Phys. Rev. B **81**, 214432 (2010).
[41] E. J. Samuelsen and G. Shirane, Phys. Status Solidi **42**, 241 (1970).
[42] S. Shi, A. L. Wysocki, and K. D. Belashchenko, Phys. Rev. B **79**, 104404 (2009).
[43] The only exception is $J_6^{Cr^{3+}\text{-}Cr^{3+}}$ which also has a large error bar indicating that this parameter could not be determined reliably possibly due to an insufficient number of spin configurations.